Journal of Materials Chemistry A

Accepted Manuscript

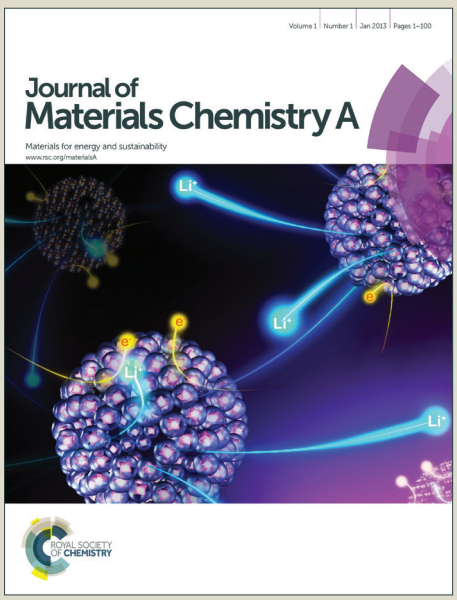

ROYAL SOCIETY OF CHEMISTRY

www.rsc.org/materialsA

Efficient Oxygen Reduction Reaction Using Mesoporous Ni-doped Co_3O_4 Nanowire Array Electrocatalysts

Xili Tong[a&], *Xinhui Xia*[c,&], *Congxiu Guo,*[a] *Yongqi Zhang,*[b] *Jiangping Tu,*[c]
Hong Jin Fan, *[b,d] *and Xiang-Yun Guo**[a]

[a] *State Key Laboratory of Coal Conversion,Institute of Coal Chemistry Chinese Academy of Sciences, Taiyuan 030001, China*

[b] *Division of Physics and Applied Physics, School of Physical and Mathematical Sciences, Nanyang Technological University, Singapore 637371*

[c] *State Key Laboratory of Silicon Materials, Key Laboratory of Advanced Materials and Applications for Batteries of Zhejiang Province, and Department of Materials Science and Engineering, Zhejiang University, Hangzhou 310027, China*

[d] *CINTRA CNRS/NTU/Thales, UMI 3288, 50 Nanyang Drive, Singapore*

[&] *Xili Tong and Xinhui Xia contributed equally to this work.*

Abstract

Catalyst for oxygen reduction reaction (ORR) is of highly industrial importance for fuel cells and metal-air battery. ORR catalysts with high electrochemical activity, selectivity, stability and low cost are extremely desirable but still remain challenging. Herein, mesoporous Ni-doped Co_3O_4 nanowire (NW) arrays are reported as a highly efficient and low-cost ORR catalyst. The Ni doping affords more electroactive sites and enhanced conductivity, and the mesoporous structure provides increased surface exposure, which may improve ion/electron transport and reduce charge transfer resistance. The NW arrays exhibit a high ORR activity with four-electron transfer reaction in alkaline media, a half-wave potential of 0.86 V vs. RHE and a superior stability to the commercial Pt (20 wt. %)/C catalyst. Our results suggest that the mesoporous Ni-doped Co_3O_4 NW arrays could be a promising ORR catalyst for fuel cells and metal-air batteries.

Keywords: Cobalt oxide; Nanowires; Electrocatalysis; Oxygen reduction reaction; Ni doping; Mesoporous structure

* Corresponding author.
E-mail address: xyguo@sxicc.ac.cn (X. Y. Guo)； fanhj@ntu.edu.sg (H. J. Fan)

1. Introduction

Fuel cells or metal-air batteries are considered as one of the most promising clean and sustainable energy technologies due to their high energy density, high efficiency, and negligible emission of harmful gases.[1] Albeit these advantages, they are still only in niche market due to, among other reasons, the foremost restriction of a sluggish oxygen reduction reaction (ORR), that requires a great deal of Pt consumption.[2] Generally speaking, key strategies to reduce Pt usage involve adopting Pt alloys with other transition metal[3-4] and optimizing Pt nanostructures.[5-6] These approaches, to some extent, can improve the utilization of Pt, but cannot completely eliminate the dependence on Pt. Therefore, low-cost alternative catalysts with high electro-catalytic activity and stability are highly desirable and are being vibrantly explored.[7-9]

Among the new alternative systems, carbon materials and 3d-transition metal oxides have sparked great interest. Typically, heteroatom-doped carbon materials (carbon nanotubes and graphene) are demonstrated with significant electro-catalytic activity for ORR.[10-11] In spite of these exciting results, the nature of catalytic sites in these carbon materials is still unclear and in debate, since the trace metal catalyst for preparation of carbon materials may also coexist in these carbon materials and play some roles in the catalytic process.[12] Meanwhile, functional carbon materials are not very stable under the fuel cell working conditions because they may be oxidized to carbon dioxide or monoxide and lose activity.[13,14] Meanwhile, in parallel with the research of carbon materials, 3d-transition metal oxides are another promising low-cost electrocatalysts with high catalytic activity, and high stability.[15,16] As one of mixed valence metal oxides, Co_3O_4 is widely investigated as a promising ORR catalysts.[17,18] It is well known that Co_3O_4 possesses spinel cubic crystal structure based on a close-packed face centered cubic configuration of O^{2-} ions, in which Co^{2+} ions occupy the one-eighth of the tetrahedral A sites while Co^{3+} ions occupy one-half of the octahedral B sites (Fig. S1). Although a bright future awaits for the Co_3O_4, the current ORR performance of pure Co_3O_4 is still not satisfactory and suffers from some issues. First, low electron transfer. The electrical conductivity of the pristine Co_3O_4 is too poor to support fast electron transfer. Second, small active surface area and few active sites. The pristine bulk Co_3O_4 catalysts generally have limited exposure of catalytically active sites and low contact area with reactants, resulting in poor ORR performance. To circumvent these problems, several strategies have been regarded promising for enhancement of ORR performance of Co_3O_4.

First, conductive composite design. The key in this approach is to combine Co_3O_4 with other conductive matrixes (such as graphene, carbon nanotubes, etc.) to improve the charge transfer rate. For example, Dai and co-workers reported that Co_3O_4 deposited on reduced graphene oxide show much enhanced ORR activity.[19] Similarly, Driess et al. prepared Co_3O_4 nanochain/carbon black (Vulcan XC-72R) composite with superior activity for ORR.[20] Second, porous nanostructure design. Porous design of Co_3O_4 is usually characterized by nanostructures such as nanowires, nanoflakes and nanoparticles. The nanostructuring has been demonstrated with large surface area and provides big contact area with O_2 and large active sites for ORR.[21] Joo et al. have shown the electrocatalytic activities of ordered mesoporous Co_3O_4 as a bifunctional catalyst for oxygen evolution reaction and ORR with high activity.[22] Third, doping effect. Doping is also an effective way to enhance the ORR performance of metal, as the heteroatom doping is expected to increase the number of catalytic active sites at the surface and the electrical conductivity. E.g., N-doped cobalt oxide nanoparticles were found to exhibit superior ORR performance to their N-free counterparts due to N doping could generate efficient catalytic sites for ORR.[23]

Due to above considerations and inspired by the previous results, we intend to combine all these strategies together into one catalytic material. Herein, we fabricate self-supported mesoporous Ni-doped mesoporous Co_3O_4 nanowires (NW) arrays as a promising earth-abundant catalyst for ORR in alkaline media. This Ni-doped Co_3O_4 NW arrays presents superior ORR catalytic activity to commercial Pt/C catalyst (20% Pt on Vulcan XC-72), and significantly better than the unmodified Co_3O_4 NWs. In addition, unlike commercial Pt/C, the obtained catalysts exhibit high tolerance to methanol and CO. It is believed that the orderly mesoporous structure endows high accessible surface areas to electrolytes and more efficient transport path for ion/electron as well as more active catalytic sites.

2. Experimental Section

Preparation of graphene foam The growth of the graphene foams was achieved by chemical vapour deposition (CVD) using Ni foams as the template. The Ni foams were put into a 5 inch quartz tube inside a horizontal tube furnace and heated to 1000 ºC under the gas flow of Ar (280 sccm) and H_2 (20 sccm) for 15 min in order to clean the surfaces of Ni foams and reduce the oxide layer. After the annealing, the temperature was reduced to 900 °C, and ethanol was bubbled into the reaction tube by Ar (160 sccm) +H_2 (40 sccm) flow under an ambient pressure. After reaction for 15 min, the tube was rapidly cooled down to room

temperature at a rate about 100 ºC min^{-1} under the protection of Ar (280 sccm) and H_2 (20 sccm). Then, the sample was immersed into a mixture solution of 2 $molL^{-1}$ $FeCl_3$ and 1 $molL^{-1}$ HCl for 5 h at 80 ºC to completely dissolve the Ni substrate to obtain graphene foam.

Preparation of Ni-doped Co_3O_4 NW arrays The reaction solution was obtained by mixing 0.1 g of $Co(NO_3)_2$, 0.02 g NH_4F and 0.1 g of $CO(NH_2)_2$ in 70 mL of distilled water and then transferred into Teflon-lined stainless steel autoclave liners in a home-made homogeneous reactor.A piece of clean Ni or graphene foam (2×4 cm^2 in sizes) was immersed into the reaction solution. The liner was sealed in a stainless steel autoclave and maintained at 110 ºC at a rotation rate of 5 cycles s^{-1} for 5 h, and then cooled down to room temperature. The samples were collected and rinsed with distilled water several times. Finally, the samples were annealed at 350 ºC in dry synthetic gas (10% O_2, 90% Ar) for 2 h to obtain self-supported Ni-doped Co_3O_4 NW arrays.

Characterizations The Ni-doped Co_3O_4 NW arrays were characterized by X-ray diffraction ((XRD; D8 Advance with Cu Kα radiation, Bruker), field emission scanning electron microscopy (FESEM, FEI SIRION). Raman spectra of the samples were recorded on a Horiba Labram HR800 spectrometer with an excitation wavelength of 633 nm. FTIR spectroscopy was carried out with a Bruker Tensor 27 spectrometer. Thermogravimetry-mass spectroscopy (TG-MS) was measured with a MS (PFEIFFER OMNI star)-TG (SETARAM SETSYS Evolution 16/18) in helium (flow rate: 100 cm^3 min^{-1}) at a heating rate of 5 K min^{-1}.The weight of Catalyst on substrate is calculated by the weight of sample reduces the weight of Ni-doped Co_3O_4 substrate. The surface area of Ni-doped NWs flaking off the substrate via ultrasonic exfoliation (KQ-700DE, 560W 30min) was determined by BET measurements using a ASAP-2010 surface area analyzer. The Ni content of the samples was measured by an inductively coupled plasma optical emission spectrometer (ICP-OES, Thermo iCAP 6300). The Co_3O_4 and Ni-doped Co_3O_4 NWs were also characterized by high-resolution transmission electron microscopy (HRTEM, JEOL JEM-20100) evaluated by X-ray photoelectron spectroscopy (XPS) performed on a Kratos XSAM 800 spectrometer using an Al Ka X-ray source.

Electrochemical measurements The electrochemical properties of each sample were tested in a beaker cell with 0.1 M KOH aqueous solution as the electrolyte using a three electrode electrochemical cell with an Ag/AgCl reference electrodeand a Pt plate (1.5 cm×1.5 cm) counter electrode with a CHI760D electrochemical workstation. The measured potentials versus the Ag/AgCl reference electrode were converted to the reversible hydrogen electrode

(RHE) scale via the Nernst equation:

$$E_{RHE} = E_{Ag/AgCl} + 0.059pH + E^{\circ}_{Ag/AgCl} \quad (1)$$

where E_{RHE} is the converted potential versus RHE, $E_{Ag/AgCl}$ is the experimental potential measured against the Ag/AgCl reference electrode, and $E^{\circ}_{Ag/AgCl}$ is the standard potential of Ag/AgCl at 25°C (0.197 V). The electrochemical measurements were carried out in 0.1 M KOH (pH = 13) at room temperature; therefore, $E_{RHE} = E_{Ag/AgCl} + 0.965$ V.

According to the method described by Dai et al.,[24] graphene foam was directly transferred onto the glassy carbon electrode (GCE 5 mm diameter, Pine) used as the working electrode, followed by casting with a Nafion solution (0.05 wt% in isopropanol) as the binder. The rotating disk electrode (RDE) was scanned cathodically at a rate of 10 mV s^{-1} with varying rotating speed from 400 rpm to 2000 rpm in O_2-saturated 0.1 M KOH electrolyte. Koutecky-Levich plots (J^{-1} vs. $\omega^{-1/2}$) were analyzed at various electrode potentials. The slopes of their best linear fit lines were used to calculate the number of electrons transferred (n) on the basis of the Koutecky-Levich equation:

$$J^{-1} = J_k^{-1} + J_L^{-1} = J_k^{-1} + B^{-1}\omega^{-1/2} \quad (2)$$

$$B = 0.2nFC_0D_0^{2/3}v^{-1/6} \quad (3)$$

$$J_k = nFkC_0 \quad (4)$$

where J is the measured current density, J_k and J_L are the kinetic- and diffusion-limiting current densities, ω is the angular velocity, n is transferred electron number, F is the Faraday constant (96485 C mol^{-1}), C_0 is the bulk concentration of O_2 (1.2×10^{-6} mol cm^{-3}), ν is the kinematic viscosity of the electrolyte (0.01 cm^2 s^{-1}), D_0 is the O_2 diffusion coefficient ($1.9\times10^{-5}cm^2$ s^{-1}), and k is the electron-transfer rate constant. For rotating ring-disk electrode (RRDE), the disk was glassy carbon and the ring is made of Pt. The ring potential was constantly set at 1.365 V vs RHE. Durability testing for the Ni-doped Co_3O_4 NW arrays and the Pt/C electrocatalysts were conducted by the chronoamperometric technique at 0.765 V vs. RHE in an O_2-saturated aqueous solution of 0.1 M KOH up to 7000 s. Electrochemical impedance spectra were measured by applying a bias of 0.765 V vs. RHE over the frequency range of 10^{-2} to 10^5 Hz with a 5 mV amplitude in Zahner electrochemical workstation.

3. Results and Discussion

The mesoporous Ni-doped Co_3O_4 NW arrays was prepared by a modified seed-mediated hydrothermal method according to our previous work.[25] XRD measurement (Fig. S2) show

that all the peaks of the precursor film on Ni foam could be well indexed to crystalline orthorhombic $Co_2(OH)_2CO_3$ (JCPDS 48-0083) (Fig. S2A). After the heat treatment, these diffraction peaks disappeared and new diffraction peaks corresponding to spinel Co_3O_4 phase (JCPDS 42-1467) was found. In the meantime, a slight shift (~0.5°, 2θ) in the diffraction peaks of Ni-doped Co_3O_4 to higher angles was observed, indicating the possible substitution of Co by Ni atoms in Ni-doped Co_3O_4 NWs. The phase of Ni-doped mesoporous Co_3O_4 NWs is also confirmed by the Raman analysis (Fig. S2) and FTIR measurement (Fig. S3). SEM images show that the whole Ni foam substrate is uniformly covered by mesoporous Co_3O_4 NWs (Fig. 1A), forming a 3D hierarchical porous structure (inset in Fig. 1A). The Ni-doped Co_3O_4 NWs have an average diameter of 70 nm and exhibit interconnected mesoporous structure with pore sizes ranging from 4 to 15 nm (Fig. 1C). Cross-sectional SEM image reveals the main length of Co_3O_4 NWs is ca. ~3 μm along the growing direction (Fig. 1D). Each Ni-doped Co_3O_4 NW has its own contact with the current collector at the bottom, which ensures that every NW participates in the ORR and provides strong adhesion and an efficient direct electron transport route. Brunauer-Emmett-Teller (BET) measurement shows that the Ni-doped Co_3O_4 NWs has a large surface area of 70.3 $m^2 g^{-1}$ with a type-IV isotherm, and the distinct hysteresis loop at a relative pressure of above 0.7 reflects the capillary condensation of the mesopores (Fig. 2A). Barrett-Joyner-Halenda (BJH) analysis further verifies the mesoporous structure with average pore size of 10 nm and gives a large pore volume of 0.23 $cm^3 g^{-1}$ (Fig. 2B). The mesopores of the Co_3O_4 NWs is ascribed to the successive release and loss of CO_2 and H_2O during the thermal decomposition of $Co_2(OH)_2CO_3$ precursor (Fig. S4). These mesopores are expected to facilitate the diffusion of reactants in ORR process and improve the exposed catalytic active sites.[26]

TEM investigations are conducted to further investigate the crystalline structure of Ni-doped Co_3O_4 NWs. As indicated in Fig. 3A, the Ni-doped Co_3O_4 NWs with the diameter of about 70 nm is composed of nanocrystallites of 10–15 nm in sizes, and many mesopores of 4–15 nm are widely distributed on the surface. The as-prepared mesoporous NWs show a crystalline selected area electron diffraction (SAED) pattern corresponding to the spinel Co_3O_4 phase. The lattice spacing of 0.467, 0.285, and 0.247 nm corresponds to the (111), (220) and (311) crystal planes of spinel Co_3O_4, respectively (Fig. 3B). The cobalt and oxygen elements are well resolved in the EDS elemental mapping and uniformly distributed at the surfaces of Ni-doped Co_3O_4 NWs (Fig. 3C-E). Sparsely distributed Ni signals are also observed, consistent with the Co and O signals (Fig. 3F). In order to check the origin of Ni

element, pure Co_3O_4 NW arrays grown on graphene foam were also prepared using the same method. It is found that there are no essential differences in morphologies of Co_3O_4 NWs between on Ni and graphene foam substrates, but no Ni element is observed in Co_3O_4 NWs on graphene foam (Fig.S5,6). Therefore, it is concluded that the Ni element comes from the Ni foam substrate. During the hydrothermal synthesis with Ni foam substrate, NH_3 is produced from decomposition of urea (see supporting information) and finally forms NH^{4+} and OH^-, which may dissolve partially the nickel foam surface and bring Ni^{2+} to the solution. Then, Ni^{2+} is proposed to co-deposit with Co^{2+} to form Ni-doped Co_3O_4 NWs. This doping phenomenon is not observed in the Co_3O_4 NWs on the 3D graphene foam, as there is no Ni source in the 3D graphene foam. Additionally, inductive coupled plasma emission spectrometer (ICP) analysis verifies that the Ni content in the Co_3O_4 NW array on Ni foam is 8.64 wt%. Based on this ratio, we purposely fabricate Ni-doped Co_3O_4 NW array on graphene foam with the same Ni percentage by adding the corresponding quantity $Ni(NO_3)_2$ into the hydrothermal reaction system.

To investigate the electro-catalytic activity, cyclic voltammogram (CV) and linear sweep voltammetry (LSV) measurements in Ar- and O_2-saturated 0.1 M KOH solutions are performed. As seen from Fig. 4A, the Ni-doped Co_3O_4 NW arrays show featureless CV within the ORR potential range in the Ar-saturated solution. In contrast, in the O_2-saturared solution, a distinct ORR peak is observed at 0.76 V, which confirms electrocatalytic activity of Ni-doped Co_3O_4 NW arrays for ORR. In addition, the current densities of Ni-doped Co_3O_4 NW arrays on Ni foam and graphene foam are almost the same height, and they both increase perfectly in step as the potential changes. Although Ni foam is welcome for commercial application due to its technical maturity and low cost, graphene foam is applied to further evaluate the electrocatalytic activity of the Ni-doped Co_3O_4 NW array for the ORR because Ni contents can be effectively controlled in the graphene foam case. Meanwhile, we also adopted other nanoscale catalysts with the same mass loading of 0.015 mg, including commercial Pt/C, Co_3O_4 NWs, Ni-doped Co_3O_4 NWs (Ni content 8.64 wt%), and graphene foam, for peer study by recording the corresponding RDE curves (1600 rpm) for ORR (Fig.4B). The half-wave potential ($E_{1/2}$) on the ORR curve is used to quickly assess the activity of a catalyst. The more positive value is $E_{1/2}$, the more active is the catalyst. Remarkably enough, Ni-doped Co_3O_4 NWs arrays exhibit a more positive $E_{1/2}$ (about 0.86 V) potential and a higher diffusion-limiting current density (about 5.76 $mAcm^{-2}$) than that of Co_3O_4 NWs (0.60 V, 1.32 $mAcm^{-2}$), graphene foam (0.71 V, 3.32 $mAcm^{-2}$) and Ni-doped

Co_3O_4 NWs (0.81 V, 4.82 $mAcm^{-2}$) and the Pt/C catalyst (about 0.85 V 5.42 $mAcm^{-2}$). Although both $E_{1/2}$ and diffusion-limiting current density of Ni-doped Co_3O_4 NW arrays are not the best values in liteature,[27,28] they are more positive than most of the reported results for non-precious metal electrocatalysts (Table S1), indicating that Ni-doped Co_3O_4 NW arrays has very high electrocatalytic activity towards ORR in alkaline medium. Additionally, Ni-doped Co_3O_4 NWs arrays also outperform in terms of the kinetic limiting current (J_k) on the basis of the RDE measurements (Fig.4C), making them as a promising substitute for commercial Pt/C catalyst at the cathode of fuel cells or metal-air batteries.

In addition to the high activity, the Ni-doped Co_3O_4 NWs array exhibits excellent stability as measured by chronoamperometric method. As seen from Fig. 4D, the ORR current density has less than 12% degradation over 7000 s, which is much better than the Pt/C catalyst (about 39% fading under the same test condition). In addition, after 4000 continuous cycles, the half-wave potential $E_{1/2}$ of Pt/C and Ni-doped Co_3O_4 NWs array exhibit a negative shift of about 80 and 30 mV, respectively (see Fig. S7). The smaller half-wave potential shift corroborates the high durability of the Ni-doped Co_3O_4 NWs array. There are nearly no changes in both the morphology and structure for Ni-doped Co_3O_4 NWs array after long-time stability testing via SEM observation (Fig. S8). However, for the Pt/C catalyst, a substantial agglomeration of Pt nanoparticles is noticed due to the Ostwald ripening, which could result in the loss of the surface and activity (Fig. S9). Therefore, the morphology and structure for Ni-doped Co_3O_4 NWs array have a positive influence on the catalyst performance decay. Its strong mechanical and morphological stability is favorable for the improvement of long-term stability.

To further evaluate the ORR performance of the Ni-doped Co_3O_4 NWs in a practical condition, the crossover effect and CO poisoning are also conducted. Strong electrochemical responses are observed for Pt/C catalyst in O_2 saturated 0.1 M KOH solution with 3M methanol and CO, respectively (Fig. 4E and F). In contrast, no obvious responses for Ni-doped Co_3O_4 NWs array are detected under the same testing conditions. These results demonstrate that, different from the commercial Pt/C, the Ni-doped Co_3O_4 NWs arrays possess high selectivity for ORR with great tolerance to possible crossover effects and CO poison, which is critical for applications in the direct methanol alkaline fuel cells.

To explore the Ni-doping effect on the ORR performance, LSV measurements with a RDE are conducted at a rotating of 1600 rpm for Co_3O_4 NWs array with different Ni-doping contents. The Co_3O_4 NWs without Ni doping exhibit much lower $E_{1/2}$ (0.74 V) and

diffusion-limited current density than those of Ni-doped Co_3O_4 samples (Fig. 5A). Since these Co_3O_4 samples possess identical nanostructures, the enhanced activity of Ni-doped Co_3O_4 samples must be attributed to the incorporation of Ni element into Co_3O_4 NWs, which results in enhanced electrical conductivity.[29] This speculation can be further supported by electrochemical impedance spectra (EIS) measurements (Fig. S10). In particular, Ni-doped Co_3O_4 NWs (n_{Ni}/n_{Co}=1:9) exhibit the most positive half-wave potential (0.86 V) and the highest diffusion-limited current density compared with other Ni-doped counterparts (n_{Ni}/n_{Co}=5:95 and n_{Ni}/n_{Co}=1:4). The aforementioned result strongly suggests that the doping level (atomic ratio between Ni and Co) plays an important role in the ORR electorcatalytic behavior. To gain further insight into electron transfer parameters for ORR in our Ni-doped Co_3O_4 NW arrays, RDE voltammetry is performed. Fig. 5B shows a series of RDE curves for Ni-doped Co_3O_4 NWs array (n_{Ni}/n_{Co}=1:9) recorded from 400 to 2000 rpm in O_2-saturated 0.1 M KOH electrolyte. These polarization curves exhibit increasing cathode current density with the rotation rate increases, which stems from shortened diffusion distance at high rotation speeds. The corresponding Koutecky-Levich (K–L) plots (Fig. 5C) show good linearity with parallelism, and the slopes remain approximately constant over the designated potential range (0.4 to 0.8 V). This indicates a first-order dependence of O_2 for the ORR in Ni-doped Co_3O_4 NWs array at different electrode potential. The electron-transfer number is then determined to be about 3.98 indicating a four-electron process toward ORR on Ni-doped Co_3O_4 NWs array, further verified by the negligible ring current for the reduction of O_2 to OH^- due to the negligible formation of HO_2^- recorded at a RRDE (Fig. 5D). These results demonstrate that the four-electron process is the dominating pathway for the ORR at the Ni-doped Co_3O_4 NW arrays.

As is well-known, the reduction of adsorbed O_2 to absorbed peroxide is the rate determining step during the ORR process for metal oxide catalysts in alkaline.[30] It is believed that Co^{3+} at the surface is generally assumed to be active catalytic sites for oxygen absorption and reduction.[31,32] To further analyze the possible involved reasons for the superior electrocatalytic activity of Ni-doped Co_3O_4 NW array (n_{Ni}/n_{Co}=1:9), the surface composition of Co_3O_4 samples are characterized by X-ray photoelectron spectroscopy (XPS). Observe that the Ni elements are incorporated into the Co_3O_4 NWs during hydrothermal synthesis and the Ni2p peak enhances with the increase of Ni content in the doped Co_3O_4 (Fig. S11). The Co2p spectrum shows a Co $2p_{3/2}$ peak around 780.2 eV with a satellite of 788.1 eV, and a $2p_{1/2}$ peak around 794.8 eV with a satellite of 804.4 eV (Fig. 6) (Ni and O XPS spectra are shown in

Fig.S12 and S13, respectively). Moreover, the ratio of Co^{3+} to Co^{2+} is calculated to be 1:1.3, 1:0.58, 1:0.5 and 1: 0.54 for the pure Co_3O_4, Co_3O_4 (n_{Ni}/n_{Co}=5:95), Co_3O_4 (n_{Ni}/n_{Co}=1:9) , and Co_3O_4 (n_{Ni}/n_{Co}=1:4), respectively. It indicates that the Co_3O_4 sample (n_{Ni}/n_{Co}=1:9) has the highest quantity of Co^{3+} species at the surface. In other words, the Ni substitution could improve the stability of Co^{3+} at the surface and high content of Ni is favorable for the enrichment of Co^{3+} at the surface of Co_3O_4 samples. Therefore, the density of Co^{3+} ion at the surface increases with the ratio of Ni and Co until it reaches a maximum at the ratio of 1:9. However, it decreases obviously when the ratio exceeds 1:9, which may be related to the fact that the morphology of Co_3O_4 starts to change form NWs to nanoplates under this condition (Fig. S14), because the nanoscale morphology also has a significant effect on the exposed density of Co^{3+}species.[33]

The above results reveal the high electro-catalytic activity and remarkable stability of the mesoporous Ni-doped Co_3O_4 NW arrays for ORR application. The high performance of the ORR catalyst can be ascribed to the mesoporous array architecture and Ni doping. Specifically, the NWs architecture and mesoporous walls shorten the transport/diffusion path for both electrons and ions, thus leading to fast kinetics. The large surfaces and inner space facilitate the contact between O_2 and electro-catalysts, providing more active sites for ORR. Furthermore, Ni doping increases the active catalytic sites at the surface of catalysts, leading to enhanced electrocatalytic activity. Finally, the NWs arrays structure possesses favorably morphological stability and high tolerance to methanol and CO.

4. Conclusion

In summary, we have demonstrated a facile method for the preparation of mesoporous Ni-doped Co_3O_4 NW arrays on different current collectors. Due to their unique composition and architecture, the Ni-doped Co_3O_4 NW array catalysts show enhanced ORR performance with more positive $E_{1/2}$ potentials and higher stability in alkaline media than commercial Pt/C and most of non-precious-metal ORR catalysts. The Ni doping is demonstrated as an effective way to the improvement of Co_3O_4 catalysts by increasing the active catalytic sites on the surface of catalysts. Our findings provide a deeper understanding of metal doping effect on ORR. The proposed design method can be extended to fabrication of other high-performance ORR catalysts.

Acknowledgements

X.T. acknowledges financial support from the National Science Foundation of Youths (21403275) and the Shanxi Province Science Foundation for Youths (2013021011-6). X.T., X, X and X.G. acknowledge financial support from the Foundation of State Key Laboratory of Coal Conversion (Grant No. J14-15-909). H. J. F thanks the financial support by MOE Tier 1 grant (RG104/14) and CAS/SAFEA International Partnership Program for Creative Research Teams. J. Tu acknowledges the support by the Program for Innovative Research Team in University of Ministry of Education of China (IRT13037) and Key Science and Technology Innovation Team of Zhejiang Province (2010R50013).

Appendix A. Supporting information

Supplementary data associated with this article can be found in the online version at http://www.

References

(1) G. Wu, K. L. More, C. M. Johnston, Zelenay, *Science* 2011, **332**, 443-447.

(2) S. Fu, C. Zhu, H. Li, D. Dua, Y. Lin, *J. Mater. Chem. A* 2015, **3**, 12718–12722.

(3) D. Wang, H.L. Xin, R. Hovden, H. Wang, Y. Yu, D.A. Muller, F.J. DiSalvo, H.D. Abruña, *Nat. Mater.* 2013, **12**, 81-87.

(4) S. Guo, D. Li, H. Zhu, S. Zhang, N.M. Markovic, V.R. Stamenkovic, S. Sun, *Angew. Chem. Int. Ed.* 2013, **52**, 3465-3468.

(5) M. Oezaslan, M. Heggen, P. Strasser, *J. Am. Chem. Soc.* 2012, **134**, 514-524.

(6) K.A. Kuttiyiel, K. Sasaki, Y. Choi, D. Su, P. Liu, R.R. Adzic, *Energy Environ. Sci.* 2012, **5,** 5297-5304.

(7) Z. Wen, S. Ci, F. Zhang, X.Feng, S. Cui, S. Mao, S. Luo, Z. He, J. Chen, *Adv. Mater.* 2012, **24**, 1399-1404.

(8) R. Silva, D. Voiry, M. Chhowalla, T. Asefa, *J. Am. Chem. Soc.* 2013, **135**, 7823-7826.

(9) D. Wang, X. Chen, D. G. Evans, W. Yang, *Nanoscale* 2013, **5**, 5312-5315.

(10)D. Yang, D. Bhattacharjya, S. Inamdar, J. Park, J. Yu, *J. Am. Chem. Soc.* 2012, **134** 16127-16130.

(11) H. Cong, P. Wang, M. Gong, S. Yu, *Nano Energy* 2014, **3**, 55–63.

(12) L. Wang, A. Ambrost, M. Pumera, *Angew. Chem. Int. Ed.* 2013, **52,** 13818-13821.

(13) N. Spătaru, X. Zhang, T. Spătaru, D.A. Tryk, A. Fujishima, *J. Electrochem. Soc.* 2008, **155,** B264-269.

(14) F. Li, D. Tang, Y. Chen, D. Golberg, H. Kitaura, T. Zhang, A.Yamada, H. Zhou, *Nano Lett.* 2013, **13**, 4702-4707.

(15) G. Zhang, B.Y. Xia, X. Wang, X.W. Lou, *Adv. Mater.* 2014, **26**, 2408-2412.

(16) S. Guo, S. Zhang, L. Wu, S. Sun, *Angew. Chem. Int. Ed.* 2012, **51,** 11770-11773.

(17) Y. Liang, H. Wang, P. Diao, W. Chang, G. Hong, Y. Li, M. Gong, L. Xie, J. Zhou, J. Wang, T.Z. Regier, F. Wei, H. Dai, *J. Am. Chem. Soc.* 2012, **134**, 15849-115857.

(18) X. Zou, J. Su, R. Silva, A. Goswami, B.R. Sathe, T. Asefa, *Chem. Commun.* 2013, **49**, 7522-7524.

(19) Y. Liang, Y. Li, H. Wang, J. Zhou, J. Wang, T. Regier, H. Dai, *Nat. Mater.* 2011, **10,** 780-786.

(20) P.W. Menezes, A. Indra, D. González-Flores, N.R. Sahraie, I. Zaharieva, M. Schwarze, P. Strasser, H.Dau, M. Driess, *ACS Catal.* 2015, **5,** 2017-2027.

(21) S. He, E. Jiang, A. Wang, L. Lu, *Angew. Chem. Int. Ed.* 2014, **53**, 1-6.

(22) Y. J. Sa, K. Kwon, J. Y. Cheon, F. Kleitzc, S. H. Joo, *J. Mater. Chem. A* 2013, **1**, 9992-10001.

(23) H. Yu, Y. Li, X. Li, L. Fan, S. Yang, *Chem. Eur. J.* 2014, **20**, 3457-3462.

(24) Y. Xue, D.Yu, L. Dai, R. Wang, D. Li, A. Roy, F. Lu, H. Chen, Y. Liu, J. Qu, *Phys. Chem. Chem. Phys.* 2013, **15**, 12220-12226.

(25) X. Xia, D. Chao, X. Qi, Q. Xiong, Y. Zhang, J. Tu, H. Zhang, H.J. Fan, *Nano Lett.* 2013, **13**, 4562−4568.

(26) X. Xia, J. Tu, Y. Zhang, X. Wang, C. Gu, X. Zhao, H.J. Fan, *ACS Nano* 2012, **6**, 5531-5538.

(27) H. T. Chung, J. H. Won, P. Zelenay, *Nat. Comm.* 2013, **4**, 1922. (DOI: 10.1038/ncomms2944)

(28) D. Yu, Y. Xue, L. Dai, *J. Phys. Chem. Lett.* **2012**, *3*, 2863-2870.

(29) Y. Li, P. Hasin, Y. Gao, *Adv. Mater.* 2010, **22**, 1926-1929.

(30) F. Chen, T. Zhang, Y. Zhang, J. Du, X. Han, J. Chen, *Angew. Chem. Int. Ed.* 2013, **52**, 2474-2477.

(31) X. Xie, Y. Li, Z. Liu, M. Haruta, W. Shen, *Nature* 2009, **458**, 746-749.

(32) J. Xu, P. Gao, T.S. Zhao, *Energy Environ. Sci.* 2012, **5**, 5333-5339.

(33) Y. Xiao, C. Hu, L. Qu, M. Cao, *Chem. Eur. J.* 2013, **19**, 14271-14278.

Figure captions

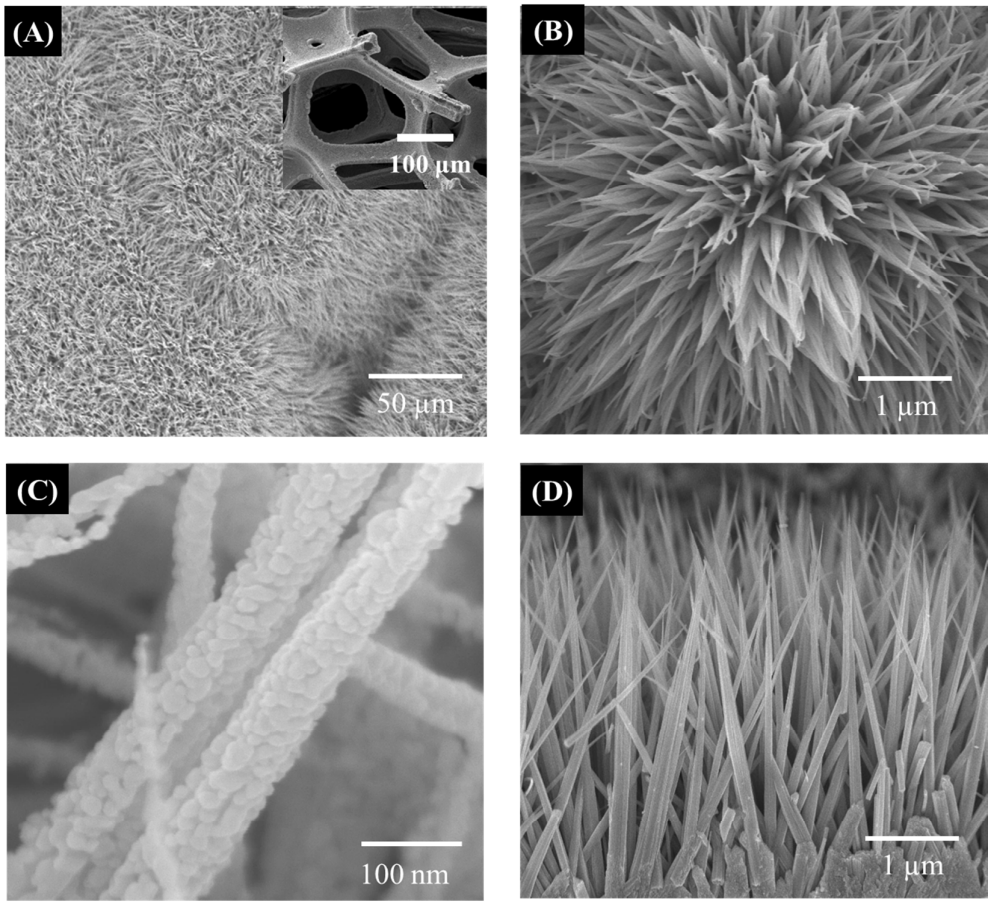

Figure 1. (A,B) Low-magnification SEM images of Ni-doped Co_3O_4 NW arrays from the top, (C) high-magnification images of Ni-doped Co_3O_4 NWs and (D) Low-magnification images of Ni-doped Co_3O_4 NWs from the side; the inset of (A) shows the 3D hierarchical porous structure

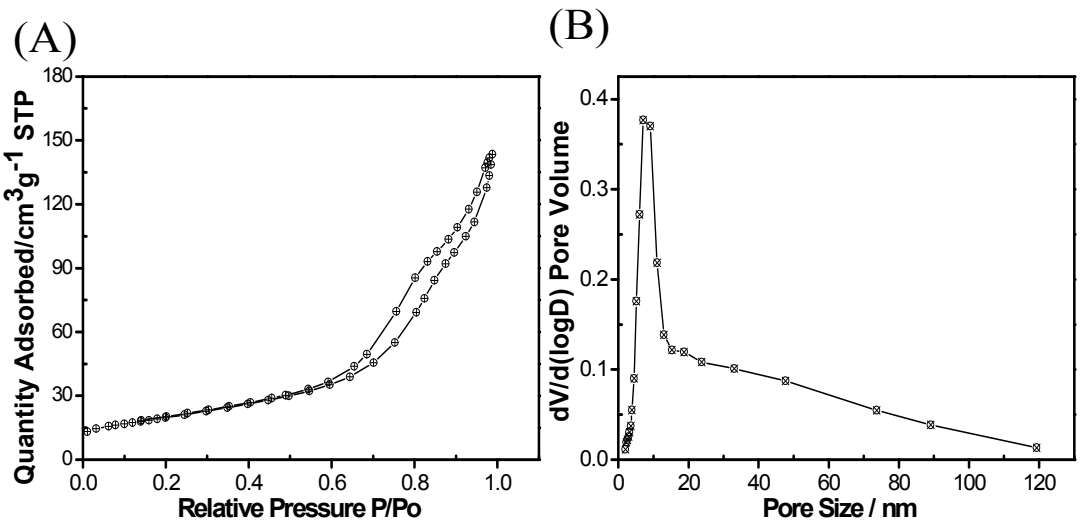

Figure 2. (A) The isothermal curve and (B) pore size distribution of Ni-doped Co_3O_4 NWs flaking off the substrate via ultrasonic exfoliation.

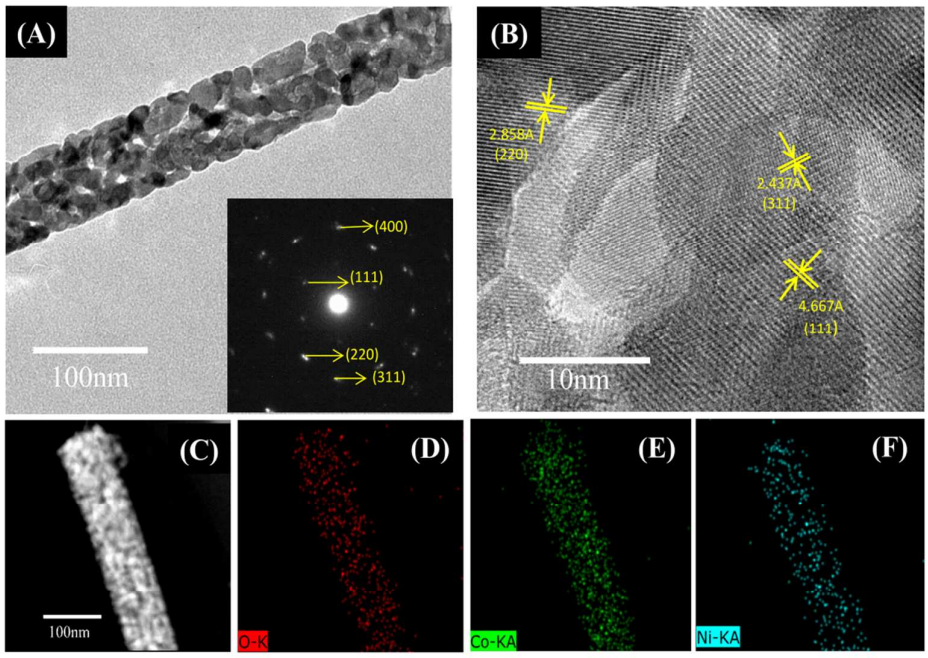

Figure 3. (A) Typical TEM (inset: SAED pattern) and (B) HRTEM of Ni-doped Co_3O_4 NW flaking off the substrate via ultrasonic exfoliation; (C) TEM image of Ni-doped Co_3O_4 NWs for element analysis, (D–F) Elemental mappings of O, Co and Ni, respectively.

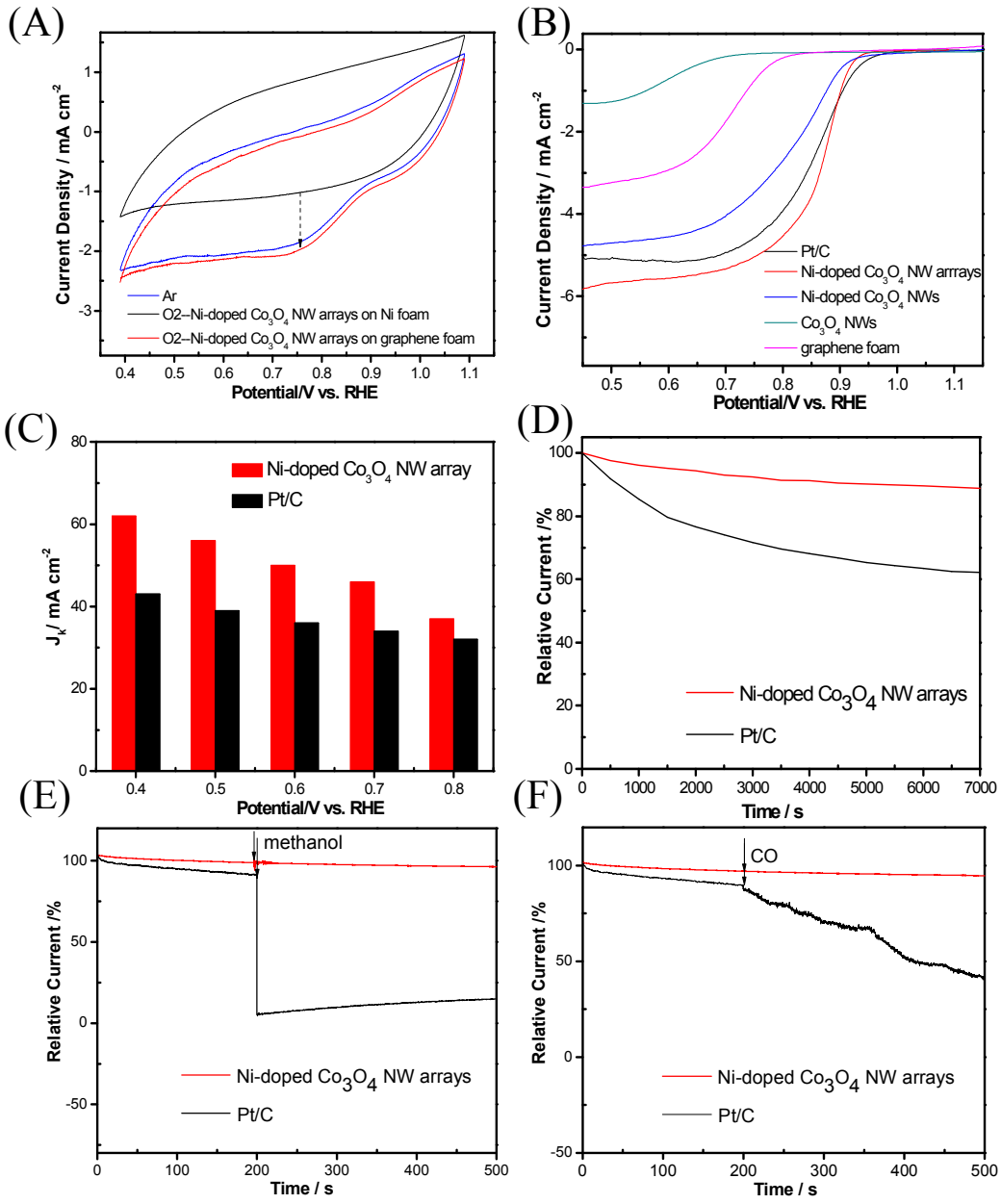

Figure 4. (A) CV curves of Ni-doped Co_3O_4 NW arrays on Ni and graphene foam at a scan rate of 50 mVs^{-1} in Ar- and O_2- saturated 0.1 M KOH; (B) RDE voltammograms at 10 $mVs^{-1}$for different electrodes in an O_2-saturated 0.1 M KOH solution at a rotation rate of 1600 rpm;(C) Electrochemical activity given as the kinetic limiting current (J_k) at 0.4, 0.5, 0.6, 0.7 and 0.8 V; (D) Chronoamperometric responses of Ni-doped Co_3O_4 NW arrays and Pt (20% Pt on Vulcan XC-72) at 0.765 V, and chronoamperometric responses of Ni-doped Co_3O_4 NW arrays and Pt/C in O_2-saturated 0.1 M KOH by adding of 3 M methanol (E) and CO (F) after about 200 s at 0.765 V.

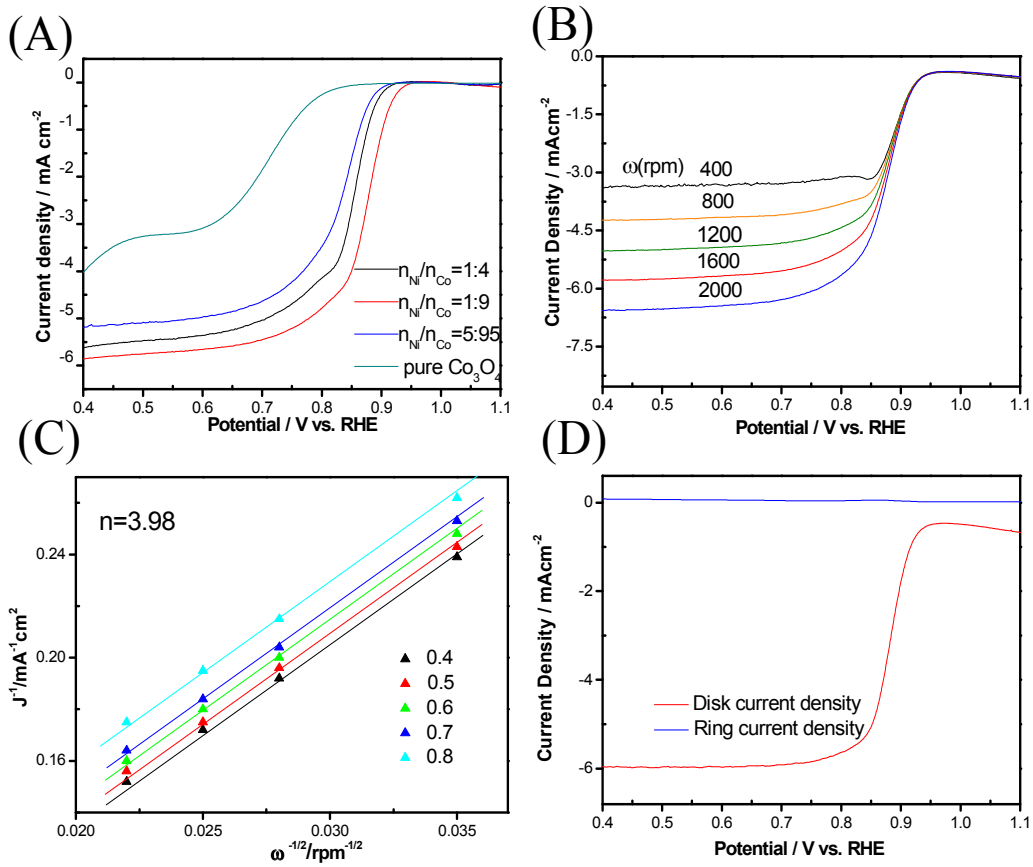

Figure 5. (A) RDE voltammograms of Ni-doped Co_3O_4 NW arrays with different Ni contents at a scan rate of 10 mVs^{-1} at a rotation rate of 1600 rpm in O_2-saturated 0.1 M KOH; (B) RDE voltammograms of Ni-doped Co_3O_4 NW arrays (n_{Ni}/n_{Co}= 1:9) at different rotation rates and at a scan rate of 10 mV s^{-1} , (C) Koutecky-Levich plot of j^{-1} versus $\omega^{-1/2}$ obtained from the RDE data in (B) at 0.4, 0.5, 0.6, 0.7, and 0.8 V in O_2-saturated 0.1 M KOH; (D) RRDE voltammograms of Ni-doped Co_3O_4 NW arrays (n_{Ni}/n_{Co}= 1:9) at a rotation rate of 1600 rpm and at a scan rate of 10 mV s^{-1} in O_2-saturated 0.1 M KOH. The ring potential was constant at 1.395 V vs RHE.

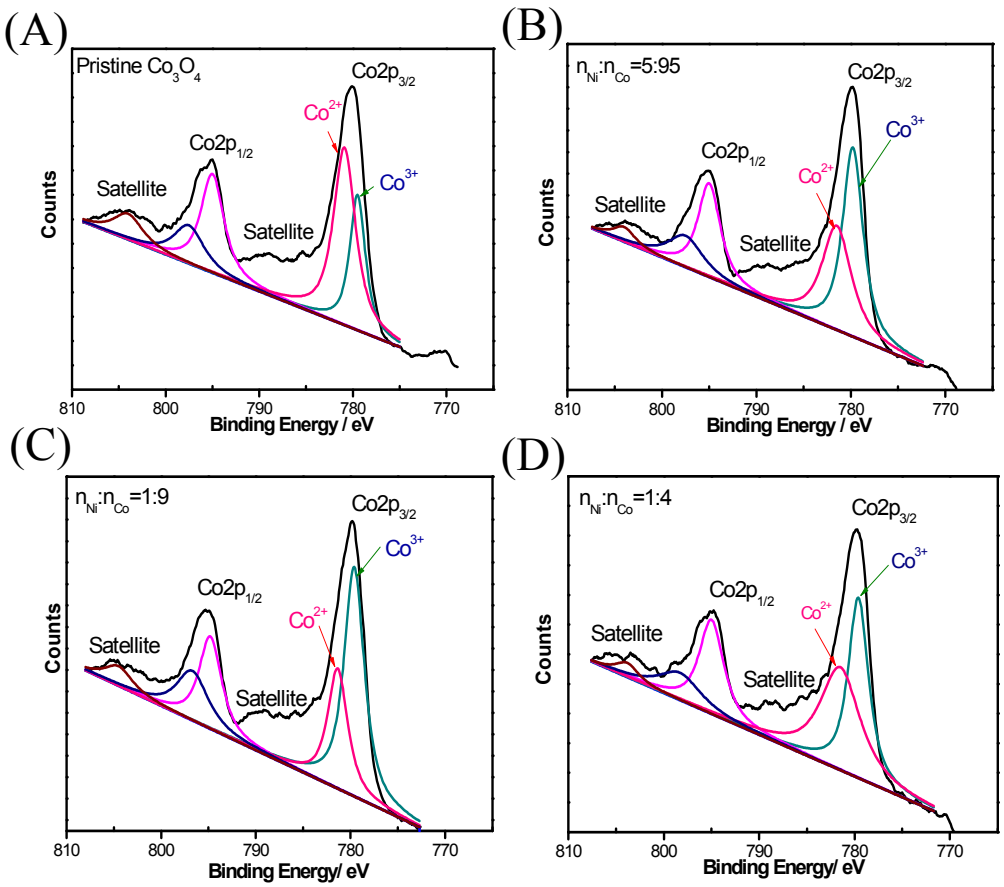

Figure 6. XPS spectra of Co element in different Co_3O_4 NWs flaking off the substrate via ultrasonic exfoliation.